On-off intermittency in an optically injected semiconductor laser

S. Osborne,[1] A. Amann,[1,2] D. Bitauld,[1,*] and S. O'Brien[1]
[1]*Tyndall National Institute, University College Cork, Lee Maltings, Cork, Ireland*
[2]*School of Mathematical Sciences, University College Cork, Ireland*
(Received 8 November 2011; published 10 May 2012)

We report on the observation of on-off intermittency in an optically injected dual-mode semiconductor laser. It is shown that quasi-single-mode chaotic dynamics of the injected mode are accompanied by intermittent and irregular bursts of the intensity of the uninjected mode. We define a threshold intensity of the uninjected mode to distinguish laminar and bursting states of the system. For small values of the threshold parameter we observe excellent agreement with the predictions of theory for the distribution of the laminar phase durations. For larger values of the threshold parameter, a gap appears in the distribution of laminar phase durations. Numerical simulations demonstrate that this gap is a consequence of the fact that in this case the on states of the system define large intensity spikes, which can belong either to the same or to distinct bursts away from the single-mode manifold.

DOI: 10.1103/PhysRevE.85.056204 PACS number(s): 05.45.−a, 42.55.Px, 42.65.Sf

I. INTRODUCTION

On-off intermittency describes a particularly striking example of dynamical behavior. In the laminar or "off" state, an observable of a dynamical system takes on small values and can remain almost constant for long periods. These laminar phases are punctuated at irregular intervals by periods of bursting dynamics, which define the "on" states of the observable [1–3].

In recent years, a wide variety of physical systems have been shown to exhibit this type of intermittent behavior. These include electrical circuits [4,5], a gas discharge plasma [6], spin-wave and liquid crystal systems [7–9], and synthetic dynamos [10]. Mathematically, on-off intermittency is associated with the onset of transverse instability of a chaotic attractor which is embedded in an invariant submanifold of a dynamical system [11,12]. On-off intermittency can also be understood as resulting from the dynamical forcing of a parameter through a bifurcation point [4,13,14]. Following from this, many experimental studies of the phenomenon included a stochastic forcing near the point of instability in order to drive the intermittent dynamics [4,8].

Here we provide an experimental and numerical study of on-off intermittency in an optically injected dual-mode semiconductor laser. It is well known that the single-mode semiconductor laser with injection exhibits a variety of complex dynamical behaviors including chaos [15]. The single mode injected system is accurately modeled in a three-dimensional phase space that describes the dynamics of the injected mode and the carrier density. With the addition of the second primary mode to the model equations, the single-mode injected system becomes an invariant submanifold of the larger dual-mode system, with the carrier density variable providing the coupling to the intensity of the uninjected primary mode. Such a system has precisely the required structure to exhibit on-off intermittency when the dynamics of the injected mode are chaotic. This is what we observe experimentally and in numerical simulations.

This paper is organized as follows. In Sec. II, we describe our device and experimental setup and provide intensity time traces characterizing the intermittent dynamics. We present a statistical analysis of the experimental results based on the distribution of time intervals between periods of bursting dynamics. Significant departures from ideal scaling are observed for large values of the threshold parameter that define the on states of the system. In Sec. III, we introduce our model equations that describe the dual-mode injected system, and we demonstrate that intermittent bursting dynamics are found in a region where the dynamics of the injected mode are chaotic. We present a statistical analysis of the dynamics, showing how the results of numerical simulations are in very good agreement with measurements. Consideration of the grouping of large intensity spikes enables us to explain the origin of the departures from ideal scaling that are observed in measured data and in numerical simulations.

II. EXPERIMENTAL RESULTS

The device we consider is a multiquantum-well InP/InGaAlAs FP laser of length 350 μm with a peak emission near 1.3 μm. It incorporates slotted regions etched into the laser ridge waveguide that determine the lasing mode spectrum. For our experiment, we adjust the device current so that the time-averaged optical power in both primary modes of the free-running laser is approximately equal. In this case the free-running device supports these two primary modes with almost 40 dB intensity contrast and a frequency detuning of 480 GHz [16]. Choosing a fixed injected power level, we vary the detuning, $\Delta\omega$, of the injected field from the long wavelength mode of the device. The optical spectra of the two primary modes are shown as a function of the frequency detuning of the injected signal in Fig. 1. If we begin in the single-mode injection locking region of the phase space at negative detuning, and move toward positive values, the device makes a transition to unstable locking, while the dynamics remain single mode. As the detuning is increased further, the device undergoes a period doubling route to chaotic dynamics.

*Current address: Nokia Research Center, 21 J J Thomson Avenue, Cambridge CB3 0FA, UK.

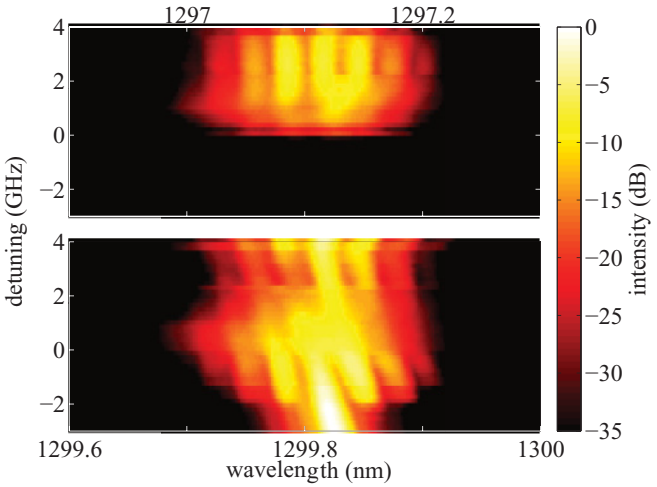

FIG. 1. (Color online) Experimental optical spectra of the dual-mode device as the frequency detuning, $\Delta\omega$, is varied at a fixed injection. Upper panel: uninjected mode. Lower panel: injected mode.

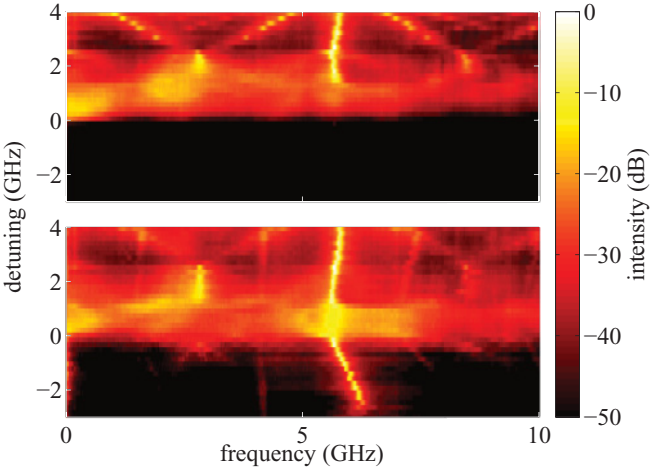

FIG. 2. (Color online) Frequency-resolved power spectral measurements of the device as the frequency detuning, $\Delta\omega$, is varied at a fixed injection. Upper panel: uninjected mode. Lower panel: injected mode.

The chaotic state is reached around zero detuning and is at first a single-mode state of the device.

However, as we increase the detuning, moving further into the chaotic region, we observe that the dynamics become two mode, with the uninjected mode experiencing irregular and intermittent bursts of intensity. Frequency-resolved measurements of the power spectral densities corresponding to Fig. 1 are shown in Fig. 2. In the lower panel of this figure one can see that the transition to unstable locking at a detuning value of -2 GHz is associated with undamping of the relaxation oscillations, with a frequency of approximately 5.5 GHz. Following this region, the weak and broadened signal at half the relaxation oscillation frequency is evidence for a period doubling bifurcation. Near zero detuning the dynamics become chaotic and are characterized by broadband spectra.

The region where we find on-off intermittent dynamics is found at small positive values of the detuning. At the onset of these dyanmics, where the intensity of the uninjected mode first becomes nonzero, the power spectrum of the uninjected mode is characteristic of a low-frequency and noiselike signal. Time traces which illustrate the dynamics in this region are shown in Fig. 3. These time traces were measured near the boundary of the region of intermittent dynamics, with the detuning in this case equal to approximately 0.5 GHz. One can see that for this value of the detuning the intensity in the uninjected mode can be dominated by spontaneous emission noise for long periods of order 100 ns. At irregular intervals, however, large-amplitude bursts of intensity are observed. These bursts can comprise single or multiple peaks or spikes of the intensity within a single bursting event. In the inset of the upper panel a bursting event which includes a single large intensity spike is shown.

On-off intermittency can be distinguished from other varieties of intermittent dynamics by considering the scaling behavior of the probability distribution of the laminar phase durations. The laminar phase duration is in our case the time between two bursts of the intensity away from the single-mode manifold. Using simple one-dimensional models, it was shown that a fundamental scaling law for the distribution of the laminar phase durations τ_L exists. This ideal scaling law is given by $P(\tau_L) \sim \tau_L^{-3/2}$, where $P(\tau_L)$ is the probability density function for the laminar phase durations [11,17]. In the presence of additive noise, a distinct shoulder appears in the distribution, which is followed by an exponential falloff for large laminar phase durations [13,14].

In the one-dimensional models of Refs. [13,14,17], scaling laws were derived by assuming a multiplicative stochastic forcing of the dynamical variable near a stability boundary. The dynamical variable in these models then represents the direction transverse to the single-mode submanifold of our system. In our case, however, the dynamics of the uninjected mode are driven chaotically, and on-off intermittency occurs where chaotic orbits in the single mode submanifold obtain a positive Lyapunov exponent for perturbations transverse to the submanifold.

In order to study the distribution of laminar phase durations we introduce a threshold parameter I_T, which the intensity of the uninjected mode must exceed in order to define the on

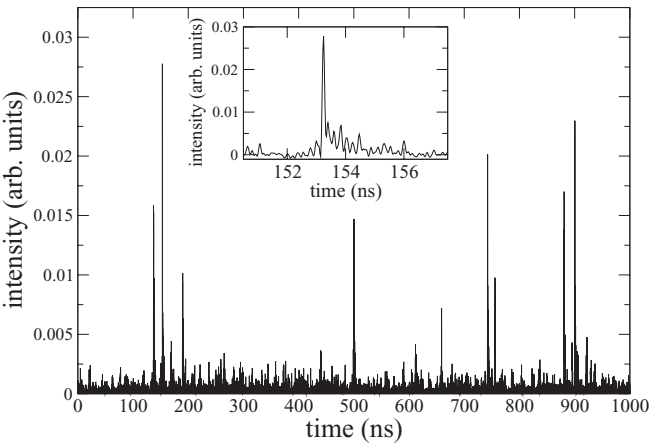

FIG. 3. Experimental time trace of the intensity of the uninjected mode of the device. An individual bursting event is shown in the inset. The frequency detuning is approximately 0.5 GHz.

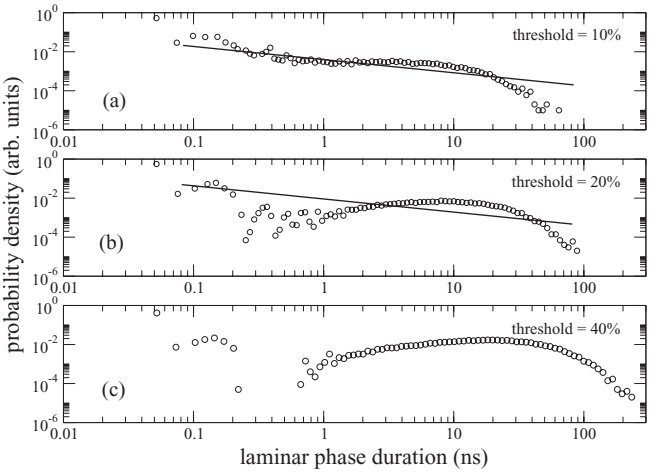

FIG. 4. Histograms of the laminar phase duration for increasing values of the threshold parameter I_T. The frequency detuning is approximately 0.5 GHz. In (a) and (b) the solid line is the $-3/2$ scaling law predicted by theory.

state of the system. For an appropriate choice of the threshold value I_T we face the following trade-off: A low I_T will lead us to record many distinct peaks of the intensity, which are actually part of the same burst away from the single-mode manifold. On the other hand, a large value of I_T will lead to the on states of the system defining large intensity spikes. In this limit we expect to encounter bursting events which do not trigger an intensity spike. For large threshold values we define τ as the time between successive events where the intensity of the uninjected mode crosses the value I_T from below. Experimentally determined histograms of the intervals τ for various threshold values I_T are shown in Fig. 4.

The data in Fig. 4(a) were obtained for a threshold value of I_T given by 10% of the time-averaged intensity in the uninjected mode. In this case, agreement with the predictions of the theory for the distribution of the laminar phases with the measured distribution is reasonably good, and we attribute this to the fact that the threshold parameter is relatively small and also because these data were obtained near the onset of the intermittent dynamics. For shorter intervals τ up to about 2 ns, we have close to $-3/2$ power-law scaling as indicated by the solid line in the figure. As τ increases, a clear shoulder region is observed where the probability distribution is in excess of the power law behavior. For $\tau > 10$ ns, an exponential falloff is observed. Departures from ideal scaling for very short intervals are also observed in this figure. As we increase the threshold value I_T in Fig. 4(b) and 4(c), the departures from ideal scaling become more significant, and for the largest threshold value a gap appears in the distribution between approximately 0.2 and 0.7 ns.

III. MODELING OF THE DEVICE RESPONSE

The rate equations that describe the dual-mode semiconductor laser with optical injection can be written in normalized units as follows:

$$\dot{E}_1 = \tfrac{1}{2}(1+i\alpha)[g_1(2n+1)-1]E_1 + \eta_1, \tag{1}$$

$$\dot{E}_2 = \tfrac{1}{2}(1+i\alpha)[g_2(2n+1)-1]E_2 + K\exp(i\Delta\omega t) + \eta_2, \tag{2}$$

$$T\dot{n} = P - n - (1+2n)\sum_m g_m|E_m|^2, \tag{3}$$

where the nonlinear modal gain is

$$g_m = g_m^{(0)}\left(1+\epsilon\sum_n \beta_{mn}|E_n|^2\right)^{-1}. \tag{4}$$

Here $|E_1|$ is the normalized amplitude of the electric field of the uninjected mode, E_2 is the normalized complex electric field of the injected mode, and n is the normalized excess carrier density. The bifurcation parameters are the normalized injected field strength K and the angular frequency detuning $\Delta\omega$. Further parameters are the phase-amplitude coupling α, the product of the carrier lifetime and the cavity decay rate T, the normalized pump current P, and the linear modal gain $g_m^{(0)}$. In our numerical simulations we used the values $\alpha = 2.6$, $T^{-1} = 0.00125$, $P = 0.5$ (twice threshold), and $g_m^{(0)} = 1$. The cross- and self-saturation are determined by $\epsilon\beta_{mn}$, and we use the values $\epsilon = 0.01$, $\beta_{12} = \beta_{21} = 2/3$, and $\beta_{11} = \beta_{22} = 1$, which allow for a stable two-mode state of the free-running device. To account for spontaneous emission noise we have added Gaussian white noise terms $\eta_1(t)$ and $\eta_2(t)$ to the dynamical equations for the fields. These equations provide excellent agreement with experimentally observed dynamics over a wide range of parameter values [18,19]. Note that although they are written symmetrically, with complex fields defined for both primary modes of the device, the phase of the uninjected mode is decoupled in these equations leading to an effectively four-dimensional system.

One can see immediately that the single-mode dynamics are contained within an invariant submanifold ($E_1 = 0$) in these equations. The system with $E_1 = 0$ is three-dimensional, describing the dynamics of the complex amplitude of the injected mode and the carrier density variable. In Fig. 5 (left panels) we plot the local extrema of the numerically calculated field intensities, $|E_1|^2$ and $|E_2|^2$, as a function of the frequency detuning. The value of the normalized injected field strength is $K = 0.008$. To locate this region of dynamics in the global bifurcation picture, see Refs. [18] and [19]. On the left of the diagram at negative frequency detuning we find an equilibrium region of stable injection locking where the uninjected mode is off. As the detuning is increased toward zero, a Hopf bifurcation occurs, and we enter the unstable locking region. Further increasing the detuning, a series of period doubling bifurcations are encountered before the dynamics of the injected mode become chaotic [15,20]. Over this detuning range the uninjected mode remains off. However, at a point inside the chaotic region, we find that the uninjected mode turns on and that its intensity envelope increases smoothly at first.

The value of the detuning where the uninjected mode turns on is approximately 0.884 GHz, which we label as $\Delta\omega^*$. This is slightly larger than the experimentally observed value and reflects the fact that the extent of the region of two-mode dynamics in the experiment of Fig. 1 is larger than that found numerically. A numerically generated time trace of the

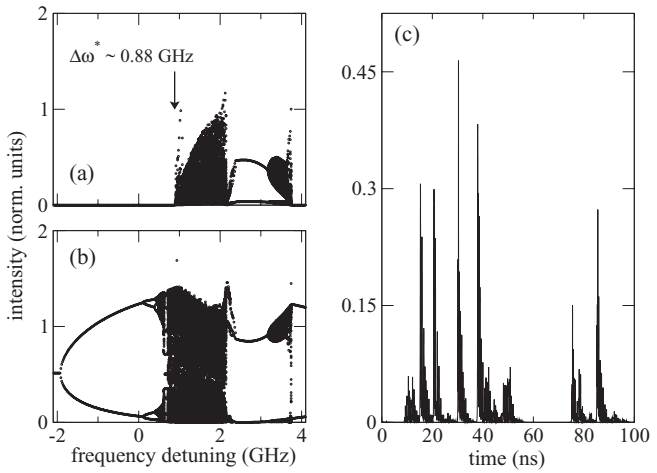

FIG. 5. Left panels: Local extrema of the field intensities (a) $|E_1|^2$ and (b) $|E_2|^2$ obtained from numerical integration of Eqs. (1)–(3) as a function of the detuning. The injected field strength is $K = 0.008$. Right panel: Numerical time traces of the dynamics of the uninjected mode. The frequency detuning is 0.89 GHz. The injected field strength is the same as in (a).

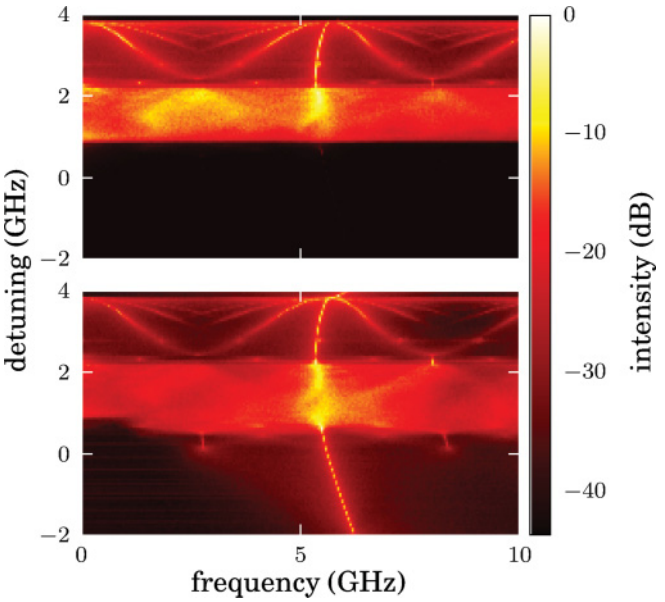

FIG. 6. (Color online) Numerically generated power spectra of the device as the frequency detuning, $\Delta\omega$, is varied at a fixed injection. The noise level is 0.002 in normalized units. Upper panel: uninjected mode. Lower panel: injected mode.

intensity of the uninjected mode of the device is shown in the right-hand panel of Fig. 5. The detuning here is 0.89 GHz, slightly larger than $\Delta\omega^*$. One can see that the intensity is switching on to large values in a quasirandom manner, and these bursts of activity can be separated by long periods where the intensity is very small. This is the characteristic behavior associated with on-off intermittency and matches closely the dynamics found in our experiment. From Fig. 5, one can see that the region of on-off intermittency is followed by a region of chaotic dynamics in both modes of the laser. This region is exited through a series of inverse period-doubling bifurcations until a dual-mode limit-cycle is found around a detuning value of 2 GHz.

Numerically generated power spectral densities corresponding to Fig. 5 are plotted in Fig. 6. Here we have included the effects of spontaneous emission noise in order to enable a comparison with experimental data. The noise level used was equal to 0.002 in normalized units, which gave good agreement with the modal intensity fluctuations in the free running device. One can see that the detuning value where significant intensity in the uninjected mode is observed is not very different from the value observed in the noise-free simulations of Fig. 5. One can also see that while the value of the detuning where the uninjected mode turns on is shifted toward a larger detuning value, the power spectrum of the uninjected mode is at first characteristic of a low-frequency and noiselike signal as was the case in the experiment.

We note also that the transition to a dual-mode limit cycle near a detuning of 2 GHz was also found in the experimental measurements of Fig. 2. As discussed in Ref. [19], the dual-mode limit cycle undergoes a torus bifurcation, which can be identified in Fig. 2 near a detuning of 2.5 GHz where a pair of frequencies are generated from the feature at one-half of the relaxation oscillation frequency. Further increasing the detuning, one of the generated frequencies decreases toward zero, leading to bursting dynamics with divergent period. This region of dynamics will be the subject of detailed study in future work.

The transition from single-mode chaotic dyanmics to on-off intermittency in our system can be understood by considering the dynamics of the amplitude of the uninjected mode explicitly. We find

$$|\dot{E}_1| = \tfrac{1}{2}[g_1(2n+1) - 1]|E_1|. \tag{5}$$

From this equation one can see that the factor $g_1(2n+1) - 1$ plays the role of the multiplicative forcing parameter for the dynamics in the transverse direction. The average value of this quantity is then the transverse Lyapunov exponent for the system, which changes sign at the point where on-off intermittency appears. In Fig. 7 we have plotted the probability density function of the forcing parameter for two values of the detuning. These data were generated by following trajectories confined to the single-mode submanifold of the governing

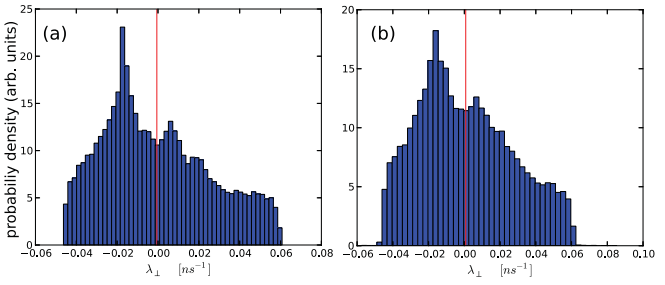

FIG. 7. (Color online) Probability density functions of the multiplicative forcing parameter, $g_1(2n+1) - 1$, for the dynamics in the transverse direction for two values of the detuning parameter. In (a) the frequency detuning is 0.87 GHz, while in (b) the frequency detuning is 0.89 GHz. The vertical line is the average value in each case.

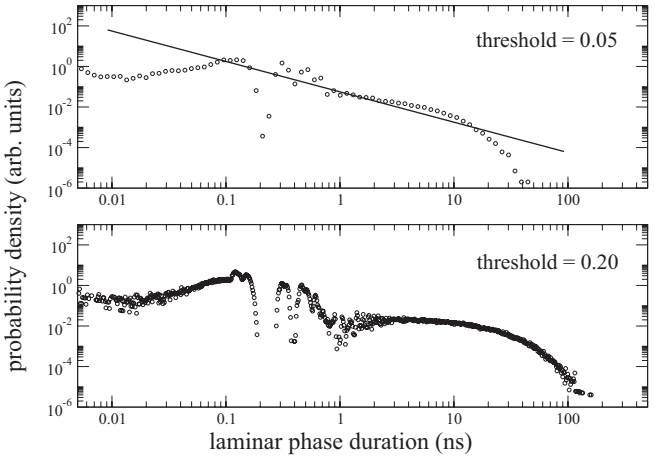

FIG. 8. Histograms of the laminar phase duration for two values of the threshold parameter I_T including spontaneous emission noise. The frequency detuning is 0.89 GHz, and the spontaneous emission noise level is 0.002 in normalized units. In the upper panel the solid line is the $-3/2$ scaling law predicted by theory.

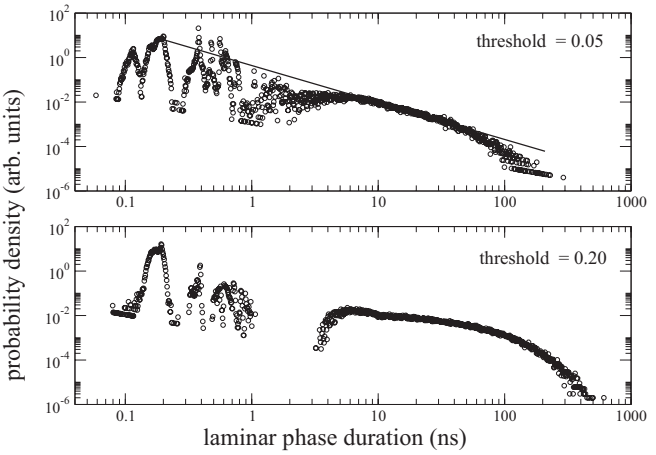

FIG. 9. Histograms of the laminar phase duration for two values of the threshold parameter I_T neglecting spontaneous emission noise. The frequency detuning is 0.89 GHz. In the upper panel the solid line is the $-3/2$ scaling law predicted by theory.

equations. One can see that the average value of this quantity changes sign near a detuning value of 0.88 GHz.

Histograms of the durations of the intervals between on states of the uninjected mode intensity are shown in Fig. 8. For these simulations we included the same level of spontaneous emission noise as in Fig. 6 in order to more closely match experimental results. In the upper panel the threshold value was set to $I_T = 0.05$ in normalized intensity units. Here the detuning is again 0.89 GHz. For this figure 100 000 peaks of the intensity were recorded. One can see that the distribution is in good agreement with the predictions of theory for the laminar phase duration. For values greater than approximately 1 ns, the distribution follows the $-3/2$ scaling. There is also a distinctive shoulder region present with a clear exponential dropoff for longer intervals. This shoulder region is centered at a similar time interval to the experimental result of Fig. 4(a). In the lower panel of Fig. 8, we have plotted the same data for $I_T = 0.2$. The time trace of Fig. 5(c) indicates that in this case on states of the system correspond to large intensity spikes, and we can see evidence for a region of forbidden values for the interspike intervals. The location of this region around 1 ns is also in qualitative agreement with experiment.

In order to illustrate more clearly the presence of the forbidden region for large threshold values I_T, in Fig. 9 we have plotted the same histograms as in Fig. 8 but without including the effects of spontaneous emission noise. We first notice that the average interval is much larger as one would expect in the absence of noise. One can also see that the data for the smaller threshold value in the upper panel are in good agreement with the theoretical scaling law over a wider range of values and that the shoulder region is not apparent as was the case for the noisy system. What is most striking is the very large forbidden region in the lower panel for larger thresholds, which now opens above 1 ns duration.

To obtain a better understanding of this forbidden region observed for large threshold values, it is useful to study the correlation between the duration τ of the time between spikes of the intensity and the minimal value of $|E_1^2|$ which is obtained between them. The corresponding scatter plot is shown in Fig. 10. We observe that there are two clusters, one at short interspike times, which is associated with relatively large minimal values of $|E_1^2|$. The dynamics associated with this cluster therefore do not return closely to the invariant manifold at $|E_1^2| = 0$. The two intensity spikes which bound this interval can therefore be interpreted as part of the same bursting event. On the other hand, there exists a second cluster in Fig. 10 located at large interspike times and small minimal values of $|E_1^2|$. Events in this cluster therefore correspond to trajectories which do return closely to the invariant manifold leading to well-separated spikes. The spikes associated with this cluster will therefore belong to separate bursting events, and therefore this cluster characterizes the interburst times or equivalently the laminar phase durations. The clear separation between the clusters in Fig. 10 and the absence of events for interspike times around 1.5 ns explains the forbidden region in the numerical interspike histogram shown in the lower panel

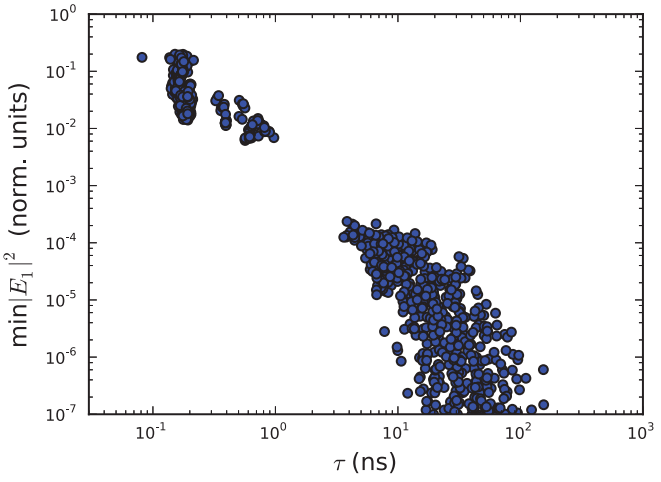

FIG. 10. (Color online) Plot of the minimum value of the uninjected field $|E_1^2|$ between two successive spike events versus the interspike interval τ. The threshold parameter is $I_T = 0.2$. All other parameters are chosen as in Fig. 9.

of Fig. 9. We argue that this mechanism is also responsible for the experimentally observed gap in the interspike histograms which appears around 0.5 ns in Fig. 4 (c).

IV. CONCLUSIONS

In conclusion, we have experimentally studied the distribution of laminar phase durations in an optically injected dual-mode laser close to the onset of on-off intermittency. We have shown that the characteristic features of this distribution agree well with numerical simulations obtained from a simple four-dimensional rate equation model. We showed in particular that the appearance of a gap in the distribution of laminar phase durations for large values of the threshold parameter could be explained by considering the grouping of large intensity spikes within single or distinct bursts of the uninjected mode intensity.

ACKNOWLEDGMENTS

This work was supported by Science Foundation Ireland. The authors wish to thank the anonymous reviewers for their constructive comments on the manuscript.

[1] H. Fujisaka and T. Yamada, Prog. Theor. Phys. **74**, 918 (1985); **75**, 1087 (1986).
[2] N. Platt, E. A. Spiegel, and C. Tresser, Phys. Rev. Lett. **70**, 279 (1993).
[3] E. Ott and J. C. Sommerer, Phys. Lett. A **188**, 39 (1994).
[4] P. W. Hammer, N. Platt, S. M. Hammel, J. F. Heagy, and B. D. Lee, Phys. Rev. Lett. **73**, 1095 (1994).
[5] Y. H. Yu, K. Kwak, and T. K. Lim, Phys. Lett. A **198**, 34 (1995).
[6] D. L. Feng, C. X. Yu, J. L. Xie, and W. X. Ding, Phys. Rev. E **58**, 3678 (1998).
[7] F. Rödelsperger, A. Čenys, and H. Benner, Phys. Rev. Lett. **75**, 2594 (1995).
[8] T. John, R. Stannarius, and U. Behn, Phys. Rev. Lett. **83**, 749 (1999).
[9] A. Vella, A. Setaro, B. Piccirillo, and E. Santamato, Phys. Rev. E **67**, 051704 (2003).
[10] G. Verhille, N. Plihon, G. Fanjat, R. Volk, M. Bourgoin, and J.-F. Pinton, Geophys. Astrophys. Fluid Dyn. **104**, 189 (2010).
[11] E. Ott, *Chaos in Dynamical Systems*, 2nd ed. (Cambridge University Press, Cambridge, UK, 2002).
[12] P. Ashwin, J. Buescu, and I. Stewart, Nonlinearity **9**, 703 (1996).
[13] N. Platt, S. M. Hammel, and J. F. Heagy, Phys. Rev. Lett. **72**, 3498 (1994).
[14] A. Čenys, A. N. Anagnostopoulos, and G. L. Bleris, Phys. Lett. A **224**, 346 (1997).
[15] S. Wieczorek, B. Krauskopf, and D. Lenstra, Opt. Commun. **172**, 279 (1999).
[16] S. Osborne, S. O'Brien, K. Buckley, R. Fehse, A. Amann, J. Patchell, B. Kelly, D. E. Jones, J. O'Gorman, and E. P. O'Reilly, IEEE J. Sel. Top. Quantum Electron. **13**, 1157 (2007).
[17] J. F. Heagy, N. Platt, and S. M. Hammel, Phys. Rev. E **49**, 1140 (1994).
[18] S. Osborne, K. Buckley, A. Amann, and S. O'Brien, Opt. Express **17**, 6293 (2009).
[19] S. Osborne, A. Amann, K. Buckley, G. Ryan, S. P. Hegarty, G. Huyet, and S. O'Brien, Phys. Rev. A **79**, 023834 (2009).
[20] V. Kovanis, A. Gavrielides, T. B. Simpson, and J. M. Liu, Appl. Phys. Lett. **67**, 2780 (1995).